Analytica Chimica Acta 1133 (2020) 48–57

Contents lists available at ScienceDirect

Analytica Chimica Acta

journal homepage: www.elsevier.com/locate/aca

Development of a new electrochemical DNA biosensor based on Eu^{3+}–doped NiO for determination of amsacrine as an anti-cancer drug: Electrochemical, spectroscopic and docking studies

Hamid Akbari Javar [a], Zahra Garkani-Nejad [b], Gholamreza Dehghannoudeh [c], Hadi Mahmoudi-Moghaddam [c, d, *]

[a] Pharmaceutics Department, Faculty of Pharmacy, Tehran University of Medical Sciences, Tehran, Iran
[b] Chemistry Department, Faculty of Science, Shahid Bahonar University of Kerman, Kerman, Iran
[c] Pharmaceutics Research Center, Institute of Neuropharmacology, Kerman University of Medical Sciences, Kerman, Iran
[d] Environmental Health Engineering Research Center, Kerman University of Medical Sciences, Kerman, Iran

HIGHLIGHTS

- Eu^{3+} -doped NiO as a novel nanocomposite was synthesized.
- An electrochemical biosensor was fabricated with new nanocomposite.
- The interaction between ds-DNA and amsacrine was studied.
- Determination of amsacrine were done by DNA biosensor in urine and serum samples.

GRAPHICAL ABSTRACT

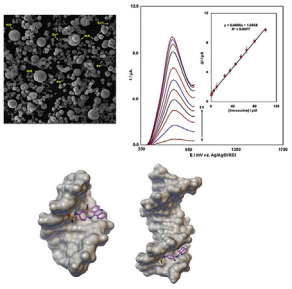

ARTICLE INFO

Article history:
Received 16 April 2020
Received in revised form
20 July 2020
Accepted 30 July 2020
Available online 12 August 2020

Keywords:
Amsacrine
Biosensor
Nanocomposite
Carbon paste electrode

ABSTRACT

The present research reported a new electrochemical biosensor based on ds-DNA/Eu^{3+} doped NiO/CPE to detect amsacrine. Therefore, UV–Vis spectrophotometry, docking, and differential pulse voltammetry (DPV) have been used to study the interactions between amsacrine and dsDNA. Then, experimental parameters affected DNA immobilization and interactions between amsacrine and ds-DNA have been optimized. Afterwards, guanine oxidation peak current of ds-DNA has been chosen as a signal to analyze amsacrine in a concentration ranging between 0.1 and 100.0 μM and finally, limit of detection (LOD) of 0.05 μM has been calculated at optimal condition. Ultimately, it was found that the suggested biosensor is able to determine amsacrine in human serum and urine samples successfully.

1. Introduction

Conducting studies on interaction of some molecules with DNA has become important for obtaining a perception of their action mode at molecular level, the origins of numerous diseases and drugs repositioning in the role of anti-cancer agents [1,2].

* Corresponding author. Pharmaceutics Research Center, Institute of Neuropharmacology, Kerman University of Medical Sciences, Kerman, Iran
E-mail address: h.mahmoudi@kmu.ac.ir (H. Mahmoudi-Moghaddam).

https://doi.org/10.1016/j.aca.2020.07.071
0003-2670/

The interaction of drug with DNA was characterized utilizing the different methods such as circular dichroism [3], fluorescence spectroscopy [4], UV–Vis spectrophotometry [5], electrophoresis [6], Fourier Transform Infrared spectroscopy (FT-IR) [7], molecular modeling techniques [8] and Resonance Raman spectroscopy [9]. Although these techniques are expensive, time-consuming and several of them indicate low sensitivity.

In the past few years, electrochemical approaches were given priority in comparison to other techniques, as a result of their highly selective, sensitive, cost-efficient, prompt and simple nature [35,36][10–13].

Amsacrine as the first medicine performing as topoisomerase II poison is a well-known anti-cancer agent entailing favorable activity towards refractory acute leukemias along with Hodgkin and non-Hodgkin lymphomas [15]. In order to assess adverse effects, toxicity, therapeutic efficiency, interactions and monitoring the concentration of amsacrine in urine and serum of patients is important. In past researches, limited methods such as HPLC and GC were documented in determining amsacrinen [16,17].

The investigations on DNA biosensors attracted a huge deal of interests in recent years because of exceptional characteristics, namely selectivity, sensitivity, cost-efficient, expeditious and simplicity [37]. Nanomaterials such as graphene, graphene oxide, carbon nanotubes, silver, gold, metal oxide and quantum dots provide well-organized and stable platforms for immobilization of DNA onto the surface of sensor [19][20,21].

Recently, NiO NPs have been considered as one of the good immobilizing matrices for biosensors. These are magnetic and have a high ratio of surface area-volume. One of the other reasons for current attention to the NiO NPs would be that they have one of the highest isoelectric points of popular metal oxide nano-materials, which would make them with constant surface charge features in a wide range of environmental pHs. Additionally, NiO NPs possess reasonable electro-catalytic activities, more capability of the electron transfer that present them as perfect substances to modify biosensors [22,23].

It is notable that rare earth elements exhibited specific features like reliable optical activities and acceptable catalytic functions; therefore, they could be used in the electric, optical, catalytic, and magnetic fields. Due to the unique properties of 4f–5d electron orbitals of the rare earth elements, researchers have been started to developing the novel nanocomposite by doping rare earth elements with metal oxides and have used them as the electrode modifiers [25]. Therefore, europium as a rare earth element with 4f orbitals could generate a coupling between the s and d states of the host substances like NiO to improve the performance of electrode to detect the analyte [26].

Therefore, in this study we constructed Eu^{3+} doped NiO as a novel nanocomposite and used it for modification of carbon paste electrode.

Moreover, we used a carbon paste electrode modified with Eu^{3+} doped NiO nanocomposite and ds-DNA as a highly sensitive DNA label-free biosensor for the determination of amsacrine in biological samples. For this purpose, the effects of dsDNA immobilization time, dsDNA concentration, interaction time and amsacrine concentrations on the electrochemical response of guanine were investigated. After the successful interaction of the amsacrine with the dsDNA, a decrease in guanine oxidation signals were used as an analytical tool for determination of amsacrine. The results showed interaction of ds- DNA and amsacrine leads to more preconcentration of amsacrine in ds-DNA/Eu^{3+} doped NiO/CPE and improve the detection limit of proposed method. Moreover, the interaction between the ds-DNA and amsacrine were evaluated by other techniques such as spectrophotometry method and docking tool which confirmed the effective interaction between amsacrine and ds-DNA.

2. Experimental

2.1. Material and methods

It is notable that Metrohm with 797 VA Computrace 1.3.1 software has been used to perform the electrochemical investigation. Each measurement has been done at room temperatures. Consequently, a UV-1800 spectrophotometer (Shimadzu: Japan) has been utilized to obtain the UV–vis absorption spectra.

Sigma-Aldrich has been chosen to purchase the double-stranded fish sperm DNA (dsDNA), amsacrine hydrochloride and europium (III) chloride hexahydrate. In addition, Merck has been selected to receive $NiCl_2 \cdot 6H_2O$ and graphite powder. All of the materials were of analytical grade with high purity. The molecular docking procedure, UV–Vis spectroscopic and preparation of real samples have been described in supplementary information data part.

2.2. Synthesis of Eu^{3+} doped NiO nano composite

In this stage, 0.546 g cetyl trimethylammonium bromide (CTAB) has been dissolved in 40 mL distilled water shaking for 10 min. After that, 0.01 g europium (III) chloride hexahydrate, 0.300 g urea, and 0.475 g $NiCl_2 \cdot 6H_2O$ have been dissolved in the obtained mixed solution at moderate agitating for 30 min. Then, the solution has been transported to a 50 mL Teflon-lined steel autoclave and stored at 160 °C for 8 h. Upon the natural cooling, centrifuging has been done to collect the blue precipitate and distilled water and absolute ethanol have been used to wash it 3 times. Afterwards, it dried at 60 °C for 12 h. Ultimately, Eu^{3+} doped NiO nanocomposite have been gained via sintering the precipitate at 500 °C for 2 h under air atmosphere. The NiO NPs were prepared using mentioned method without the addition of europium (III) chloride hexahydrate [27].

2.3. Electrode preparation

For preparing carbon paste electrodes (CPEs), 0.5 g of the paste has been procured using a mix of 0.45 graphite powder and paraffin oil (0.8 ml). In the next stage, paste has been firmly pressed into a 3-mm (i.d) glassy tube and the copper wire has been placed in it from the opposite end of the tube for acting as a conductor. Moreover, CPEs surfaces have been smoothed by rubbing their external surfaces on a piece of paper prior to utilization. Then, the modified CPEs such as NiO NPs/CPE and Eu^{3+} doped NiO/CPE have been procured with a similar procedure and addition of 0.05 gr of NiO NPs and 0.05 gr of Eu^{3+} doped NiO for two electrodes respectively.

2.4. Immobilization of ds-DNA on the modified CPE surface

Notably, for immobilization of ds-DNA at the surface of Eu^{3+} doped NiO/CPE, the modified CPE has been immersed in the stirred 15.0 mg/L ds-DNA, and potential equal to +0.50 V has been applied for 250 s. Afterwards, acetate buffer solution (pH 4.8) has been utilized to wash the dsDNA-modified CPE (ds-DNA/Eu^{3+} doped NiO/CPE) for removing unbonded ds-DNA. Next, ds-DNA/Eu^{3+} doped NiO/CPE has been immersed in 0.5 M acetate buffer solution (pH = 4.8) and potential has been scanned between +600 and + 1000 mV for recording the oxidation currents of the guanine.

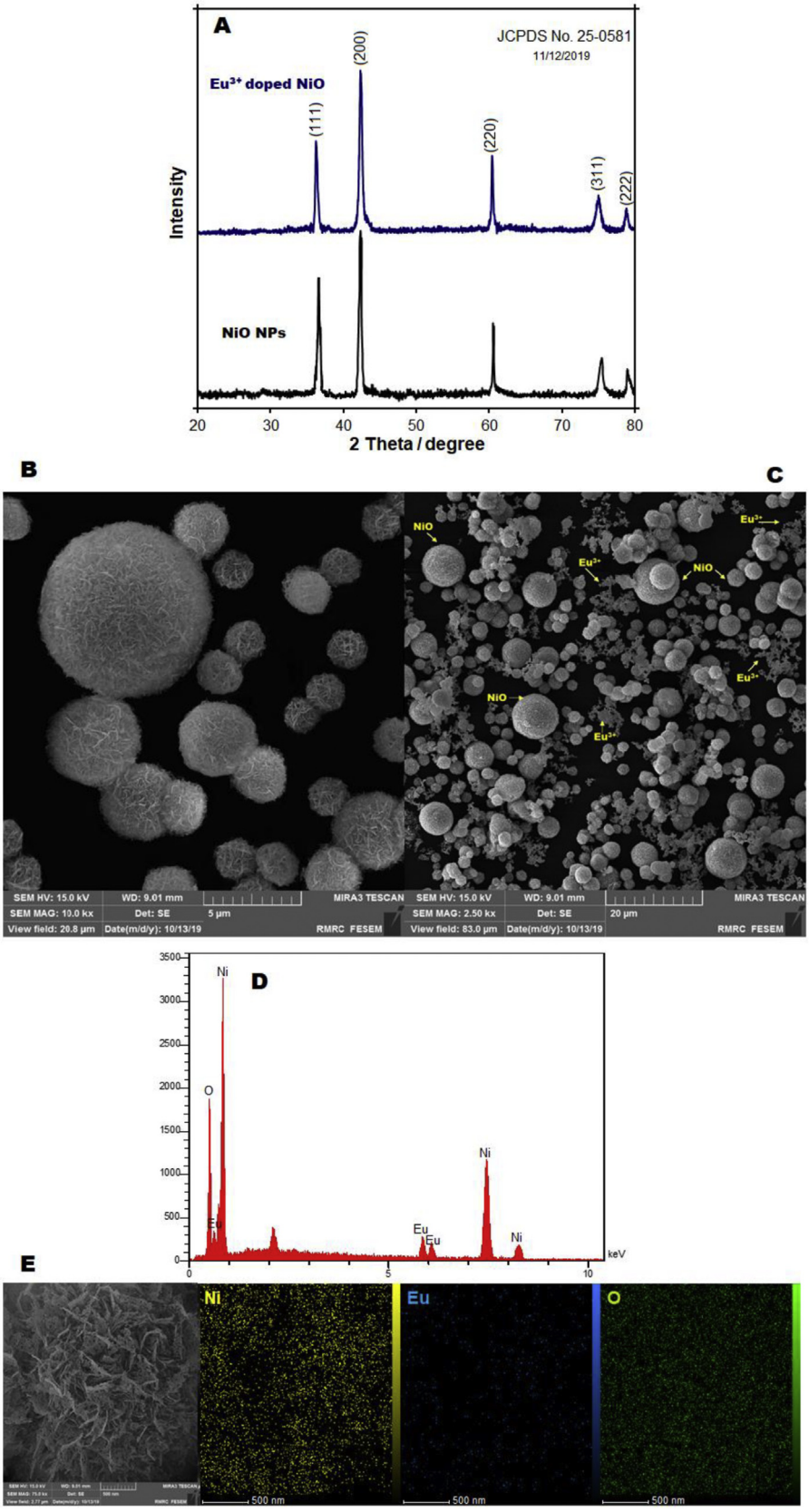

Fig. 1. A) XRDs of NiO NPs and Eu^{3+}–doped NiO, B) SEM images of NiO NPs and C) Eu^{3+}–doped NiO, D) EDS spectrum and (E) EDS mapping for Eu^{3+}– doped NiO nanocomposite.

3. Results and discussion

3.1. Nanocomposite characterization

It is notable that powder XRD has been used to examine the detailed crystal structure data of the synthesized nanocomposite. According to the XRD pattern in Fig. 1A, five major peaks of the Eu^{3+}-doped NiO at 2θ values of 37.3°, 43.2°, 62.4°, 75.4°, and 79.1° that respectively has been corresponded to the crystallographic planes of (111), (200), (220), (311), and (222) and could be completely indexed to NiO standard spectrum (JCPDS, No. 04-0835). Additionally, typical peaks of impurities could not be distinguished that has been clearly confirmed crystalline NiOs have been substantially synthesized through the facile hydrothermal procedure. The two procured Eu^{3+}-doped NiO and NiO nanocrystals (Fig. 1A) exhibited a similar phase matched completely with NiO standard spectrum, representing ineffectiveness of the Eu^{3+} substitution in the crystalline structure of the NiO NPs; therefore, Eu^{3+} ions have been substantially and smoothly doped into NiO NPs host lattice.

Furthermore, crystallite size of NiO nanocrystals have been approximated from greater intense peak of the XRD pattern (200) with Debye Scherer's equation (1);

$$D = 0.9\lambda/\beta \cos\theta \quad (1)$$

where D stands for average crystal size, λ refers to the X-ray radiation wave-length and β represents the complete width at half maximum (FWHM). Finally, the computed crystallite size from the intense plane of (200) was 12.7 nm.

In addition, scanning electron microscopy (SEM) shows morphologies of the NiO NPs in Fig. 1B which have spherical structure and the nano-sphere shell has been made of multiple porous plates. Moreover, the SEM image of Eu^{3+}-doped NiO in Fig. 1C displays, all NiO NPs have retained their spherical shape, and europium has been uniformly dispersed between these nano-spheres.

It should be noted that energy dispersive spectroscopy (EDS) has been utilized to perform the element analysis of the Eu^{3+}-doped NiO and detect the element distribution in the selected micro areas. Through the EDS spectrum, presence of Eu^{3+}, Ni, and oxygen could be observed without impurity (Fig. 1D). According to the Eu^{3+}-doped NiO EDS mapping images (Fig. 1E), Eu^{3+}, Ni, as well as oxygen have been the composites of the synthesized product.

3.2. Electrochemical characterization of the Eu^{3+} doped NiO/CPE

In this stage, the cyclic voltammograms of $Fe[CN]_6^{3-/4-}$ redox couple as one of the indicators for immobilizing DNA have been recorded at the surface of the bare CPE, NiO NPs/CPE, Eu^{3+}-doped NiO/CPE and ds-DNA/Eu^{3+}-doped NiO/CPE. Based on the outputs presented in Fig. 2, redox peaks current and reversibility at NiO NPs/CPE (curve b) enhanced as compared with the unmodified electrode (curve a). Such a condition might be due to the accelerated transfer of electron and larger surface areas of the NiO/CPE, resulting in the greater current responses. At the Eu^{3+}-doped NiO/CPE (curve c), ΔE_p declined and the peak current increased significantly on comparison with CPE and NiO/CPE. The results may be ascribed to synergic effect of Eu and NiO which is caused the increasing of modified electrode performance such as fast electron transfer rate, good antifouling property and high conductivity.

Following the DNA immobilization at Eu^{3+}-doped NiO/CPE

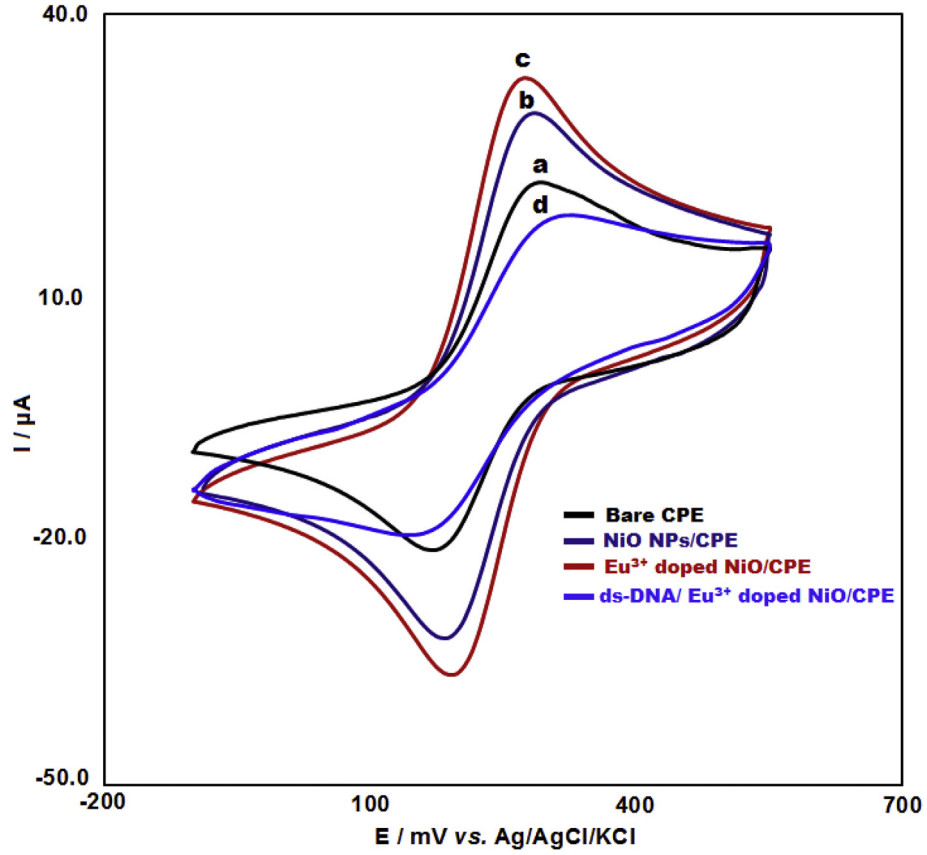

Fig. 2. (A) Cyclic voltammograms of 5 mM $[Fe(CN)6]^{3-/4-}$ in 0.1 M KCl: (a) CPE, (b) NiO/CPE (c) Eu^{3+}–doped NiO/CPE, (d) ds-DNA/Eu^{3+}– doped NiO/CPE. Scan rate: 50 mV/s.

surface, the two cathodic and anodic peak currents notably declined as the peak-to-peak potential separation enhanced (curve d). Results showed the resistance of the phosphate groups with negative charge of the immobilized DNA to the access of redox couple to the electrode and besides this electrostatic repulsion, the immobilized ds-DNA can also act as a physical blocker for electron transfer; therefore, the current would be declined [37]. The above findings demonstrated DNA immobilization at the Eu^{3+}-doped NiO/CPE surface.

3.3. Optimization of DNA immobilization

For preparing DNA biosensor, variables such as accumulation time and ds-DNA concentration on accumulation of ds-DNA at the Eu^{3+}-doped NiO/CPE surface have been examined with regard to guanine oxidation peak as an index. Therefore, for achieving the most acceptable concentration of ds-DNA, multiple concentrations of DNA in a range between 2.0 and 30.0 mg/L have been selected and outputs confirmed the greatest guanine current of 15.0 mg/L of DNA in comparison to other concentrations (Fig. S1A). Hence, this concentration has been chosen to construct ds-DNA Eu^{3+}-doped NiO/CPE. In addition, effects of the deposition time has been examined in ranges between 50 and 350 s. Results indicated increase of the oxidation peak current of guanine with the deposition time of 250 s and levelling by additional enhancement of the deposition time, which represented a saturated adsorption of ds-DNA (Fig. 1B). With regard to analysis efficiency and sensitivity, optimum deposition time of 250 s would be utilized for additional experimentations.

3.4. Study of interaction of guanine and amsacrine at the surface of the sensor

The effect of amsacrine-guanine interaction have been electrochemically investigated in comparison to the alterations in the guanine oxidation peak in the absence and presence of amsacrine. So, we registered DPV signal by means of the ds-DNA/Eu^{3+} doped NiO/CPE in the absence (curve a) and the presence of 5.0, 30.0 and 50.0 μM amsacrine (curve b, c and d respectively) (Fig. 3). According to the curve a, ds-DNA/Eu^{3+} doped NiO/CPE generated the oxidation current signal of 10.0 μA relative to guanine oxidation in ds-DNA. It should be noted that in the presence of 5.0, 30.0 and 50.0 μM amsacrine, we observed that the oxidation current has been reduced to 8.7, 6.5 and 4.0 μA, respectively, supporting interaction between amsacrine and guanine base in the ds-DNA structure. Generally, negative shifts found in the peak potential have been corresponding to the electrostatic binding, whereas the positive shifts found in the peak potential have been corresponding to the intercalation [28]. According to Fig. 3, DPVs of the ds-DNA-amsacrine complex displayed a partial positive shift in the guanine peak potential with the enhancement of amsacrine concentration. Therefore, this behavior could be attributable to intercalations of amsacrine with ds-DNA.

3.5. Effect of incubation time of amsacrine on the guanine signals

Determining the influences of the interaction time of amsacrine and ds-DNA on the guanine oxidation signal demonstrated that as the accumulation time enhanced by 350 s, the guanine peak

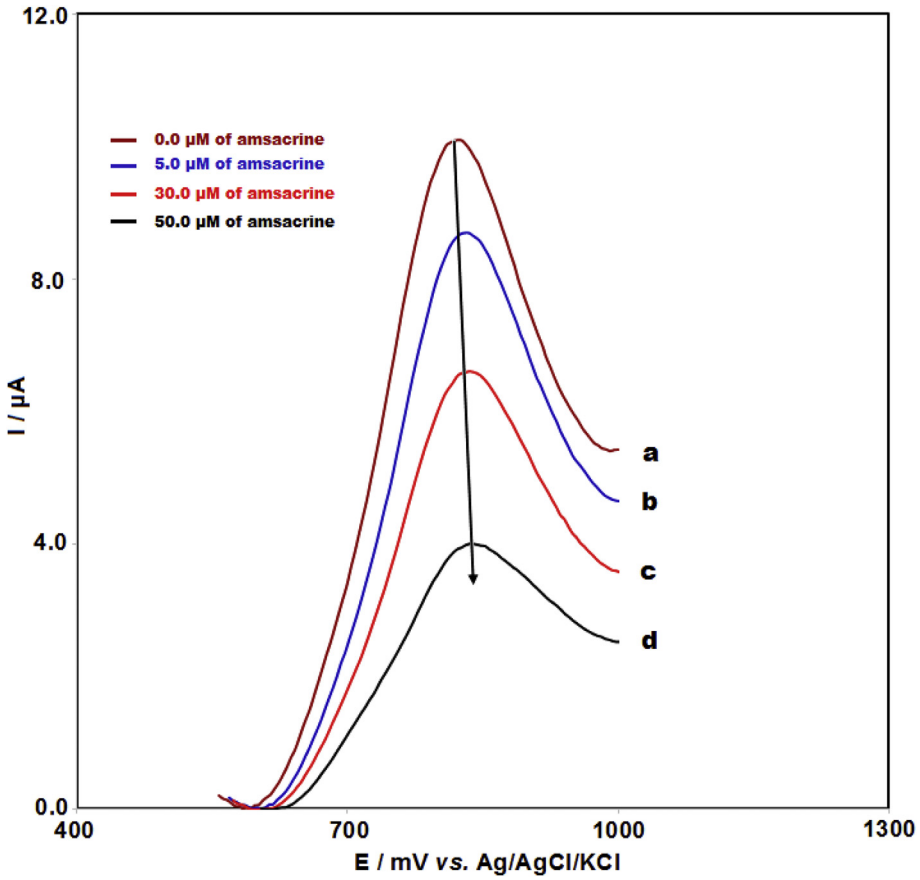

Fig. 3. Differential pulse voltammograms of guanine after the interaction between 0.0, 5.0, 30.0 and 50.0 μM amsacrine (curves a-d, respectively) and ds DNA at ds-DNA/Eu^{3+} doped NiO/CPE.

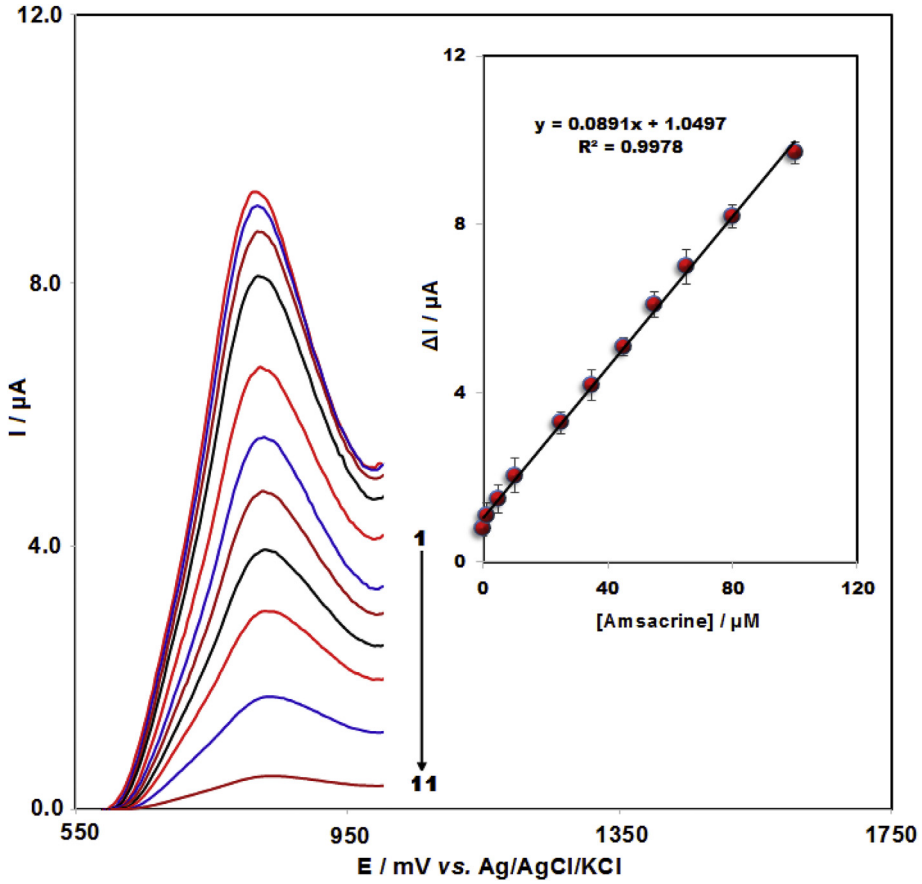

Fig. 4. Voltammograms of ds-DNA/Eu^{3+} doped NiO/CPE for different concentrations of amsacrine in phosphate buffer (0.1 M, pH 7.0). From top to bottom (1-11), 0.1, 1.0, 5.0, 10.0, 25.0, 35.0, 45.0, 55.0, 65.0, 80.0 and 100.0 µM. Inset: Dependence of the net oxidation guanine current (different between guanine current in the absence and presence of amsacrine) vs. concentration of amsacrine.

notably declined to 300 s and then it has been nearly leveled off (Fig. S2). Hence, 300 s has been confirmed as an optimum interaction time.

3.6. Linear range and LOD

DPV has been utilized to detect amsacrine concentration (Fig. 4). As seen, ΔI plot (difference between the guanine current in the absence and presence of amsacrine) versus the amsacrine concentration have been linear in ranges between 0.1 and 100.0 µM (Fig. 4- inset). In addition, LOD was calculated 0.05 µM. Table 1 compared functions of the designed biosensor and performance of the formerly published methods, confirming the wider linear range and lower LOD of the introduced procedure in comparison to some techniques. Therefore, ds-DNA/Eu^{3+}-doped NiO/CPE has been considered to be one of the effective sensing platforms.

3.7. Examination of selectivity

In the presence of 10.0 µM amsacrine, impacts of the foreign species on the guanine signals, as listed in Table S1, have been examined by DPV to assess the sensor selectivity. Moreover, the highest interfering material concentration leading to an error under ±5% for guanine detection has been defined as the tolerance limit. Outputs approved that up to a 550-fold excess of uric acid, citrate, sucrose, epinephrine, ascorbic acid, folic acid, dopamine, and L-tyrosine and 400-fold excess of K^+, Cl^- and Ca^{2+} did not affect guanine oxidation current (Fig. S3). Hence, ds-DNA/Eu^{3+}-doped NiO/CPE biosensor has reasonable selectivity to detect amsacrine.

3.8. Stability, reproducibility, and repeatability

The developed sensor could be employed to detect 50 µM amsacrine for ten times in one day with reasonable RSD value equal to 2.23% that confirmed repeatability of the sensor. In addition, the biosensor reproducibility has been addressed. Therefore, 5 DNA biosensors have been procured for detection of the 50.0 µM amsacrine. It has been found that RSD of the measurements for 5 electrodes has been 3.1%, showing the satisfactory of electrode reproducibility. Moreover, the biosensor stability has been separately examined during four weeks by means of one biosensor. It is notable that the attained values did not show any distinctive alterations (RSD 3.8%). Therefore, such an acceptable stability could be ascribed to the firm attachment of DNA sequences over the surface of Eu^{3+}-doped NiO/CPE.

Table 1
Performance comparison of different methods for determination of amsacrine.

Method	LOD	Linear range	Ref.
GC	50.0 ng/ml	–	[17]
HPLC	–	20.0–2000.0 ng/ml	[16]
HPLC	50.0 µM	0.1–10.0 µM	[33]
Electrochemistry	0.3 µM	0.7–100.0 µM	[34]
Electrochemistry	0.05 µM	0.1–100.0 µM	This work

Table 2
Analytical results of spiked amsacrine in human serum and urine (n = 5).

Sample	Added (μM)	Found (μM)	Recovery (%)	RSD (%)
Serum	-	N.D	–	–
	3.0	3.1	103.3	3.0
	9.0	9.2	102.2	1.7
	12.0	11.7	97.5	2.6
Urine	-	N.D	–	–
	5.0	5.2	104.0	1.9
	10.0	9.8	98.0	2.2
	15.0	14.8	98.6	3.3

3.9. Analyzing the real samples

In this stage, human serum and urine samples with the use of ds-DNA/Eu^{3+}-doped NiO/CPE on the basis of a standard addition procedure have been investigated to test functional utility of the introduced technique. Certain content of amsacrine has been used to spike the serum and urine samples and DPV has been performed to determine its content. Table 2 reports the outputs. As seen, recovery values ranged between 98.0% and 104.0% that were satisfactory, representing a potent utilization of the designed biosensor for detecting amsacrine in the real samples.

3.10. UV–Vis spectrophotometry

The amsacrine absorption peak appeared at about 265 nm, which was close to the absorption peak of dsDNA at 260 nm. Fig. 5 is a UV–Vis absorption spectra recorded for a constant concentration of dsDNA (15 μM) in the presence and absence of diverse concentrations of amsacrine (5–25 μM). As seen, a peak at 260 nm has been found in the absorption spectrum of free dsDNA, which has been the result of absorbtion of pyrimidine and purine in DNA. By increasing amsacrine concentration added to the constant concentration of dsDNA, due to exposing pyrimidine and purine bases of DNA, absorbance intensity of the dsDNA peak enhanced. In fact, alterations in the absorption spectrum for dsDNA could be ascribed to forming amsacrine-dsDNA complex and this form of interaction leads to slight changes in DNA conformation.

The binding constant of DNA with drug can be determined by applying the Benesi-Hildebrand equation (2) [29]:

$$\frac{A_0}{A-A_0}=\frac{\varepsilon_G}{\varepsilon_{H-G}-\varepsilon_G}+\frac{\varepsilon_G}{\varepsilon_{H-G}-\varepsilon_G}\times\frac{1}{K\,[Drug]}$$

where A_0 and A are the corresponding absorbance of ds-DNA in the absence and presence of amsacrine, respectively. ε_G and ε_{H-G} are their respective molar absorbance coefficients. Fig. 5-inset showed a good linear dependence of $A_0/(A-A_0)$ on the reciprocal amsacrine concentrations. According to the intercept to slope ratio obtained from the linear plot, binding constant of the amsacrine–DNA complex was found to be $K = 1.55 \times 10^4$/M. Furthermore, obtained K values were found comparable with the binding constant of well-known intercalators such as quercetin (3.19×10^4/M), proflavine (2.32×10^4/M), epirubicin (3.4×10^4/M) and lumazine (1.74×10^4/M) [30].

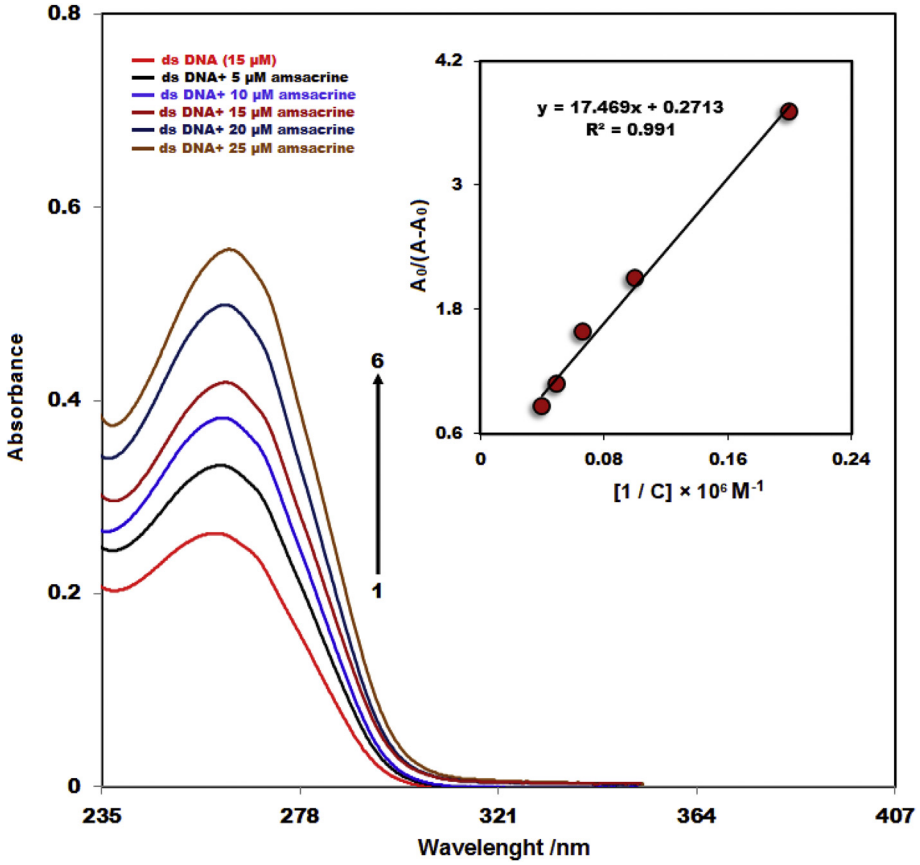

Fig. 5. UV–vis absorption spectra of ds DNA (15 μM) in the absence and presence of the amsacrine in the range of 5.0–25.0 μM. Inset: $A_0/A\text{-}A_o$ vs. 1/[Amsacrine] plot.

3.11. Docking examination

3.11.1. Minor groove docking investigation

For studying the groove interaction, a canonical DNA (PDB code: 1BNA) has been chosen to position the docking in the minor groove (Fig. 6A) and the blind docking has been run on the DNA duplex [31] and the binding energy has been obtained −7.1 kcal/mol. Studies indicated stabilization of amsacrine at the DNA minor groove (Fig. 6B). Moreover, the major contribution of hydrogen bonds has been demonstrated in interacting between amsacrine and DNA.

Hydrogen bonds included: Hydrogen (H) 3 and 22 of guanine 114 (DG114) interacted with oxygen (O) 27 from amsacrine (bond length: N-H···O 2.75 & 2.25 Å. bond angle: 129.97 & 146.89° respectively). Then, H 41 of amsacrine interacted with O 4′ from guanine 116 (DG116) (bond length: N-H···O 2.06 Å; bond angle: N-H···O 155.04). H 40 of amsacrine and O′3 from guanine 116 (DG111) (bond length = N-H···O 2.14 Å, bond angle: N-H···O 137.46°).

In addition, sulphur atom (25) of amsacrine exhibited a π interaction with aromatic ring of guanine 114 (DG 114) (bond length: 5.9 Å). C′5-H in DA111 and DG 112 established a hydrogen bond with N 7 and O 22 in amsacrine (bond length: C-H···N & C-H···O 3.39, & 3.01 Å respectively).

According to the results of docking, amsacrine can interact effectively with bases in the minor groove of DNA.

3.11.2. Intercalation docking investigation

In this stage, a conducted intercalation DNA complex (PDB code: 1Z3F) has been utilized to examine amsacrine-DNA interaction. It has been selected with regard to the published studies [32]. Therefore, the docking outputs showed stabilization of amsacrine in the intercalating location of DNA (major groove) across 2 π-loan pair interactions and 5 hydrogen bonds with the nucleotides (Fig. 6C). Based on the result, the binding energy has been estimated to be −8.0 kcal/mol. Interactions are presented here. H 41 of amsacrine interacted with O 4′ and O 2 from cytosine 55 (DC55) (bond length: N-H···O 2.10 & 3.05 Å, bond angle: N-H···O 122.79° &

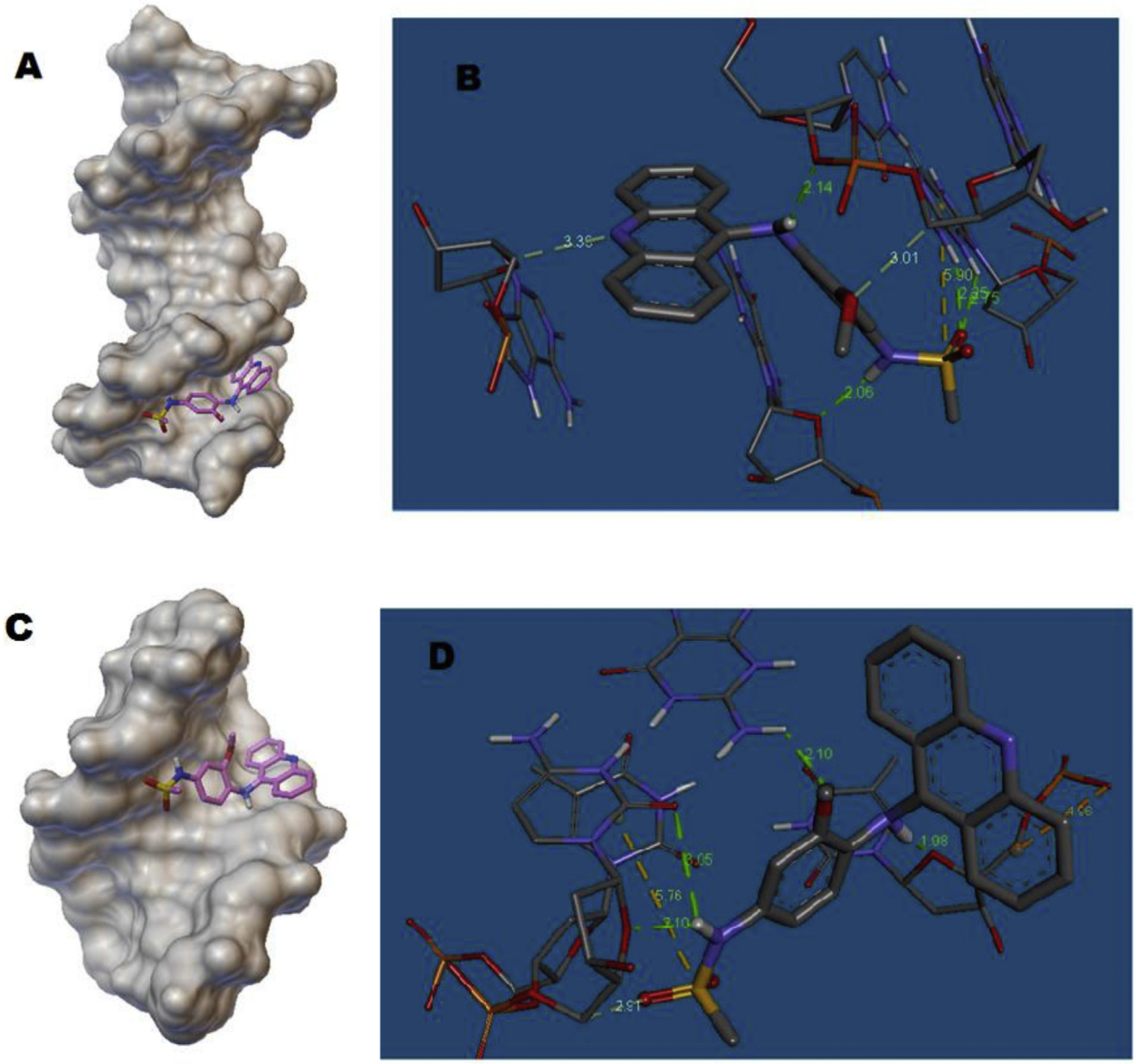

Fig. 6. (A) Amsacrine- DNA minor groove interaction. (B) Geometrical disposition of amsacrine in DNA minor groove (distances in Å). (C) Amsacrine- DNA major groove interaction. (D) Geometrical disposition of amsacrine in DNA intercalation (distances in Å).

126.0°, respectively). H 40 of amsacrine established a hydrogen bond with O 4′ of thymine 44 (DT 44) (bond length: N-H···O 1.98 Å, bond angle: N-H···O 163.45°). In addition, H 22 of guanine 22 interacted with O 22 of amsacrine (bond length: N-H···O 2.10 Å, bond angle: N-H···O 149.58°). Finally, C5′-H showed a hydrogen bond with O 27 of amsacrine (bond length: C-H···O 1.91 Å, bond angle: C-H···O 151.26°). Moreover, two π interactions like the loan pair of S 25 of amsacrine and aromatic ring of thymine 44 (DT 44) and OP1 of thymine 44 and aromatic ring of amsacrine with bond length 5.76 and 4.96 Å have been observed respectively (Fig. 6D).

Therefore, amsacrine as an intercalator has the effective interaction with DNA at the major groove that π interactions play a key role. Also, the ΔG for major groove binding is less than ΔG for minor groove interaction of amsacrine and DNA, therefore possibility of intercalation at major groove is higher than minor groove.

4. Conclusion

The present study examined amsacrine interaction with the ds-DNA using the electrochemical, UV–Vis spectrophotometry and docking techniques. The results indicated the effective interaction of amsacrine at minor and major grove of ds-DNA. In addition, the development of a selective electrochemical biosensor was conducted using Eu^{3+}-doped NiO nanocomposite and ds-DNA to determine amascrine in real specimen. Moreover, new biosensor showed acceptable repeatability and stability for detecting amsacrine with an extensive linear range from 0.1 to 100.0 μM, low LOD (0.05 μM, S/N = 3), and reasonable selectivity in presence of interferences. Based on the results, ds-DNA/Eu^{3+}-doped NiO/CPE could be utilized to detect amsacrine in the biological samples.

CRediT authorship contribution statement

Hamid Akbari Javar: Supervision. **Zahra Garkani-Nejad:** Software. **Gholamreza Dehghan Noudeh:** Formal analysis. **Hadi Mahmoudi-Moghaddam:** Conceptualization, Methodology, Investigation, Resources, Writing - review & editing.

Declaration of competing interest

The authors declare that they have no known competing financial interests or personal relationships that could have appeared to influence the work reported in this paper.

Appendix A. Supplementary data

Supplementary data to this article can be found online at https://doi.org/10.1016/j.aca.2020.07.071.

References

[1] M. Shabbir, I. Ahmad, H. Ismail, S. Ahmed, V. McKee, Z. Akhter, B. Mirza, Pharmacological, electrochemical and drug–DNA interaction aspects of tridentate Schiff bases and their triphenylphosphine nickel(II) complexes, Polyhedron 133 (2017) 270–278, https://doi.org/10.1016/j.poly.2017.05.046.
[2] M. Hasanzadeh, N. Shadjou, Pharmacogenomic study using bio- and nanobioelectrochemistry: drug-DNA interaction, Mater. Sci. Eng. C 61 (2016) 1002–1017, https://doi.org/10.1016/j.msec.2015.12.020.
[3] E. Kiss, A. Mirzahosseini, Á. Hubert, A. Ambrus, L. Őrfi, P. Horváth, DNA binding of sunitinib: spectroscopic evidence via circular dichroism and nuclear magnetic resonance, J. Pharmaceut. Biomed. Anal. 150 (2018) 355–361, https://doi.org/10.1016/j.jpba.2017.12.004.
[4] M. Sirajuddin, S. Ali, A. Badshah, Drug-DNA interactions and their study by UV-Visible, fluorescence spectroscopies and cyclic voltametry, J. Photochem. Photobiol. B Biol. 124 (2013) 1–19, https://doi.org/10.1016/j.jphotobiol.2013.03.013.
[5] R. Hajian, P. Hossaini, Z. Mehrayin, P.M. Woi, N. Shams, DNA-binding studies of valrubicin as a chemotherapy drug using spectroscopy and electrochemical techniques, J. Pharm. Anal. 7 (2017) 176–180, https://doi.org/10.1016/j.jpha.2017.01.003.
[6] M.M. Silva, E.O.O. Nascimento, E.F. Silva, J.X. de Araújo, J.C.C. Santos, I.M. Figueiredo, J.X. de Araújo, C.C. Santana, L.A.M. Grillo, R.S. de Oliveira, C.D. Buarque, P. Costa, Interaction between bioactive compound 11a-N-tosyl-5-deoxi-pterocarpan (LQB-223) and Calf thymus DNA: spectroscopic approach, electrophoresis and theoretical studies, Int. J. Biol. Macromol. 96 (2017) 223–233, https://doi.org/10.1016/j.ijbiomac.2016.12.044.
[7] E.Y. Jie, M.S. Ahn, Y.P. Lee, S.K. Sung, B.W. Min, J.R. Liu, S.W. Kim, Rapid discrimination of CMS cybrid lines between Brassica oleracea var. capitata and Raphanus sativus L. using Fourier transform infrared (FT-IR) spectroscopy of genomic DNA, Plant Biotechnol. Rep. 12 (2018) 217–228, https://doi.org/10.1007/s11816-018-0486-7.
[8] H. Mahaki, H. Tanzadehpanah, O.K. Abou-Zied, N.H. Moghadam, A. Bahmani, S. Salehzadeh, D. Dastan, M. Saidijam, Cytotoxicity and antioxidant activity of Kamolonol acetate from Ferula pseudalliacea, and studying its interactions with calf thymus DNA (ct-DNA) and human serum albumin (HSA) by spectroscopic and molecular docking techniques, Process Biochem. 79 (2019) 203–213, https://doi.org/10.1016/j.procbio.2018.12.004.
[9] M. Olszówka, R. Russo, G. Mancini, C. Cappelli, A computational approach to the resonance Raman spectrum of doxorubicin in aqueous solution, Theor. Chem. Acc. 135 (2016) 1–15, https://doi.org/10.1007/s00214-015-1781-9.
[10] H. Beitollahi, H. Mahmoudi-Moghaddam, S. Tajik, S. Jahani, A modified screen printed electrode based on La 3+ -doped Co 3 O 4 nanocubes for determination of sulfite in real samples, Microchem. J. 147 (2019) 590–597, https://doi.org/10.1016/j.microc.2019.03.031.
[11] D. Chen, M. Zhang, M. Ma, H. Hai, J. Li, Y. Shan, A novel electrochemical DNA biosensor for transgenic soybean detection based on triple signal amplification, Anal. Chim. Acta 1078 (2019) 24–31, https://doi.org/10.1016/j.aca.2019.05.074.
[12] S. Gürsoy, N. Dükar, Y.T. Yaman, S. Abaci, F. Kuralay, Electroactive polyglycine coatings for nanobiosensing applications: label-free DNA hybridization, DNA-Antitumor agent interaction and antitumor agent determination, Anal. Chim. Acta 1072 (2019) 15–24, https://doi.org/10.1016/j.aca.2019.04.044.
[13] S. Tajik, H. Mahmoudi-Moghaddam, H. Beitollahi, Screen-Printed electrode modified with La 3+ -doped Co 3 O 4 nanocubes for electrochemical determination of hydroxylamine, J. Electrochem. Soc. 166 (2019) B402–B406, https://doi.org/10.1149/2.0491906jes.
[15] K. Yamamoto, T. Kokubun, K. Sato, T. Akaishi, A. Shimazaki, M. Nakamura, Y. Shiga, S. Tsuda, K. Omodaka, H. Saya, T. Nakazawa, The DNA topoisomerase II inhibitor amsacrine as a novel candidate adjuvant in a model of glaucoma filtration surgery, Sci. Rep. 9 (2019) 1–10, https://doi.org/10.1038/s41598-019-55365-7.
[16] P.P.T. Brons, J.M.C. Wessels, P.C.M. Linssen, C. Haanen, P.A.J. Speth, Determination of amsacrine in human nucleated hematopoietic cells, J. Chromatogr. B Biomed. Sci. Appl. 422 (1987) 175–185, https://doi.org/10.1016/0378-4347(87)80450-4.
[17] A. Emonds, O. Driessen, E.A. de Bruijn, A.T. van Oosterom, Gas-chromatographic determination of amsacrine (AMSA) in plasma, Fresenius' Z. für Anal. Chem. 307 (1981) 286–287, https://doi.org/10.1007/BF00496170.
[19] M. Khater, A. de la Escosura-Muñiz, D. Quesada-González, A. Merkoçi, Electrochemical detection of plant virus using gold nanoparticle-modified electrodes, Anal. Chim. Acta 1046 (2019) 123–131, https://doi.org/10.1016/j.aca.2018.09.031.
[20] Z. Sun, L. Wang, S. Wu, Y. Pan, Y. Dong, S. Zhu, J. Yang, Y. Yin, G. Li, An electrochemical biosensor designed by using Zr-based metal-organic frameworks for the detection of glioblastoma-derived exosomes with practical application, Anal. Chem. 92 (2020) 3819–3826, https://doi.org/10.1021/acs.analchem.9b05241.
[21] B. Dinesh, A.T.E. Vilian, C.H. Kwak, Y.S. Huh, R. Saraswathi, Y.K. Han, The facile and simple synthesis of poly(3,4ethylenedioxythiophene) anchored reduced graphene oxide nanocomposite for biochemical analysis, Anal. Chim. Acta 1077 (2019) 150–159, https://doi.org/10.1016/j.aca.2019.05.053.
[22] M. Carbone, A. Nesticò, N. Bellucci, L. Micheli, G. Palleschi, Enhanced performances of sensors based on screen printed electrodes modified with nano-sized NiO particles, Electrochim. Acta 246 (2017) 580–587, https://doi.org/10.1016/j.electacta.2017.06.074.
[23] A.F. Mulaba-Bafubiandi, H. Karimi-Maleh, F. Karimi, M. Rezapour, A voltammetric carbon paste sensor modified with NiO nanoparticle and ionic liquid for fast analysis of p-nitrophenol in water samples, J. Mol. Liq. 285 (2019) 430–435, https://doi.org/10.1016/j.molliq.2019.04.084.
[25] H. Huang, J.J. Zhu, The electrochemical applications of rare earth-based nanomaterials, Analyst 144 (2019) 6789–6811, https://doi.org/10.1039/c9an01562k.
[26] M. Khairy, C.E. Banks, A screen-printed electrochemical sensing platform surface modified with nanostructured ytterbium oxide nanoplates facilitating the electroanalytical sensing of the analgesic drugs acetaminophen and tramadol, Microchim. Acta 187 (2020) 126, https://doi.org/10.1007/s00604-020-4118-x.
[27] R. Miao, W. Zeng, Q. Gao, Hydrothermal synthesis of novel NiO nanoflowers assisted with CTAB and SDS respectively and their gas-sensing properties, Mater. Lett. 186 (2017) 175–177, https://doi.org/10.1016/j.matlet.2016.09.127.
[28] A. Khodadadi, E. Faghih-Mirzaei, H. Karimi-Maleh, A. Abbaspourrad, S. Agarwal, V.K. Gupta, A new epirubicin biosensor based on amplifying DNA interactions with polypyrrole and nitrogen-doped reduced graphene:

experimental and docking theoretical investigations, Sensor. Actuator. B Chem. 284 (2019) 568–574, https://doi.org/10.1016/j.snb.2018.12.164.
[29] M.H. Nasir, E. Jabeen, R. Qureshi, F.L. Ansari, A. Shaukat, A. Ahmed, Investigation of redox mechanism and DNA binding of novel 2-(x-nitrophenyl)-5-nitrobenzimidazole (x = 2, 3 and 4), Biophys. Chem. 258 (2020), 106316, https://doi.org/10.1016/j.bpc.2019.106316.
[30] S.I. Farooqi, N. Arshad, P.A. Channar, F. Perveen, A. Saeed, F.A. Larik, A. Javeed, Synthesis, theoretical, spectroscopic and electrochemical DNA binding investigations of 1, 3, 4-thiadiazole derivatives of ibuprofen and ciprofloxacin: cancer cell line studies, J. Photochem. Photobiol. B Biol. 189 (2018) 104–118, https://doi.org/10.1016/j.jphotobiol.2018.10.006.
[31] M. Mehdipour, G. Dehghan, R. Yekta, M. Hanifeh Ahagh, M. Mahdavi, Z. Ghasemi, Z. Fathi, DNA-binding affinity, cytotoxicity, apoptosis, cell cycle inhibition and molecular docking studies of a new stilbene derivative, Nucleos Nucleot. Nucleic Acids 38 (2019) 101–118, https://doi.org/10.1080/15257770.2018.1498517.
[32] M. Medjedović, A.R. Simović, D. Ćoćić, M. Milutinović, L. Senft, S. Blagojević, N. Milivojević, B. Petrović, Dinuclear ruthenium(II) polypyridyl complexes: mechanistic study with biomolecules, DNA/BSA interactions and cytotoxic activity, Polyhedron 178 (2020), 114334, https://doi.org/10.1016/j.poly.2019.114334.
[33] J.W. Paxton, Determination of the anti-cancer drug amsacrine in biological fluids by HPLC, in: Drug Determ. Ther. Forensic Context, Springer, 1984, pp. 201–209, https://doi.org/10.1007/978-1-4613-2397-6_25.
[34] H.M. Moghaddam, H. Beitollahi, G. Dehghannoudeh, H. Forootanfar, Electrochemical determination of amsacrine at a ds-DNA modified graphene carbon paste electrode and its application as a label-free electrochemical biosensor, Int. J. Electrochem. Sci. 12 (2017) 9958–9971, https://doi.org/10.20964/2017.11.39.
[35] H.M. Moghaddam, Electrocatalytic determination of carbidopa and acetaminophen using a modified carbon nanotube paste electrode, Int. J. Electrochem. Sci. 6 (2011) 6557–6566.
[36] H.M. Moghaddam, M. Malakootian, H. Beitollah, P. Biparva, Nanostructured base electrochemical sensor for determination of sulfite, Int. J. Electrochem. Sci. 9 (2014) 327–341.
[37] H.M. Moghaddam, H. Beitollahi, G. Dehghannoudeh, H. Forootanfar, A Label-Free Electrochemical Biosensor Based on Carbon Paste Electrode Modified with Graphene and ds-DNA for the Determination of the Anti-Cancer Drug Tamoxifen, J. Electrochem. Soc. 164 (2017) B372–B376, https://doi.org/10.1149/2.0561707jes.